Supplement of Biogeosciences, 15, 2691–2722, 2018
https://doi.org/10.5194/bg-15-2691-2018-supplement

Biogeosciences Open Access EGU

Supplement of

Year-round simulated methane emissions from a permafrost ecosystem in Northeast Siberia

Karel Castro-Morales et al.

Correspondence to: Karel Castro-Morales (kcastro@bgc-jena.mpg.de)

Supplementary material

Section 1. TOPMODEL description

In the TOPMODEL approach, the position of the local water table depth (z_i) is calculated as:

$$z_i = \bar{z} + \frac{1}{f}(\chi_i - \bar{\chi}) \quad \text{(S1)}$$

Where $\bar{z}$ is the grid cell mean water table, χ_i is a local compound topographic index (CTI), $\bar{\chi}$ is the grid cell mean CTI, and f is the exponential decay of transmissivity with depth that sets the dependence of flooding on water table variation. The CTI is the main input parameter for TOPMODEL (Kirkby, 1975), and represents a topographic profile that is used to define how likely a landscape point is to become water saturated and is defined as $\gamma_i = \ln(\alpha_i / \tan \beta_i)$, where α_i is a dimensionless index used to determine the source contributing area at point i, and $\tan \beta_i$ is the local slope. Based on statistical information of the CTI, areas in a landscape with similar CTI values will have similar hydrological responses allowing a simplification of the hydrological calculations in the model. We use a global data of CTI values at a resolution of 15" by Marthews et al. (2015) to a gamma function approximation (Sivapalan et al., 1987), allowing us to reconstruct the CTI distribution for each model grid cell.

Section 2. Modifications to JSBACH-methane module

The original JSBACH-methane module presented in Kaiser et al. (2017), underwent several modifications. These are:

i) **Improved description of the plant-mediated transport**: Instead of constraining the methane transport by the root length of gas transporting vascular plants, in this model configuration the gas transported through plants is constrained by the fraction of soil volume occupied by plants roots, i.e. the root volume. This modification was done to avoid the possible use of unrealistic values for mean accumulated root lengths that are difficult to assess from field studies. In this new configuration, the actual volume of the soil that is occupied by roots (V_r) is calculated from the available pore space in the soil (i.e. (1- v_p), where v_p is the volumetric soil porosity), and the prescribed principal fraction of the pore-free soil volume filled by roots (R_{fr}), which in turn is constrained by the soil type. In the same way, and as in the original JSBACH-methane model, plant roots are modeled as one cylinder per plant tiller. Thus, the surface area that the plant roots exhibit per layer depth (A_{rl}, in m^2/m^2) within the rooting soil layers, is described as:

$$A_{rl} = \frac{4 \cdot V_r}{d_r} \quad \text{(S2)}$$

Where d_r is the diameter of an individual root, and V_r is defined as:

$$V_r = \left(1 - v_p\right) \cdot R_{fr} \cdot h \cdot \frac{LAI}{\max\left(LAI\right)} \quad \text{(S3)}$$

Where h is the soil layer height, and LAI is the varying leaf area index; thus, the last term of Eq. S2 determines the growing state of the plants. The amount of methane that is emitted through plants ($n_{plant}^{CH_4}$) remains as in Eq. 7 of Kaiser et al. (2017):

$$n_{plant}^{CH_4} = D_r^{CH_4} \cdot \left(c^{CH_4} - c_{air}^{CH_4}\right) \cdot \frac{1}{h_{exo}} \cdot \mathrm{d}t \cdot A_{rl} \cdot f_r \quad \text{(S4)}$$

Where $D_r^{CH_4}$ is the diffusion coefficient of the root exodermis for methane, which is defined as 80 % of the diffusion coefficient for CH_4 in water, D_w (i.e. $D_r = 0.8\ D_w$, where 0.8 is meant as a factor of resistance r of the root exodermis to gas transfer), c^{CH4} is the concentration of methane in the soil, $c_{air}^{CH_4}$ is the atmospheric methane concentration, h_{exo} is the thickness of the exodermis, dt is the time step, and f_r is the fraction of roots able to transport gases, which is set to ~83 % based on the same criteria of *Carex aquatilis* dominance over the dominance of total vascular plants in a square meter of wet soils, i. e. $f_r = \frac{dominance\ C.\ aquatilis}{dominance\ vasc.\ plants} = \frac{25}{30}$ (Kutzbach et al., 2004). Positive values of $n_{plant}^{CH_4}$ represent emissions of gas from the soil into the atmosphere. The formulation for oxygen uptake through plants is the same as in Eq. 6 of Kaiser et al., 2017, but with opposite sign convention (i.e. here, negative values mean uptake of gas from the atmosphere into the soil).

The transport of gas through plants is a two-way simultaneous pathway, with a flux of oxygen and methane between the atmosphere and pore spaces in the soil layers. Transport of methane through plants will take place as long as there is sufficient gas in the soil pockets to diffuse through the plant exodermis. The gradient of the gas concentrations is evaluated at every time step until it equals zero. At this point, the concentration of gas in the soil (i.e. in soil air and soil moisture combined) is equal to the so-called equilibrium concentration. That is the combined concentration in the soil air and in the soil moisture that would be in equilibrium with the concentration in atmospheric air according to Henry's Law. Thus, the magnitude of the two-way plant-mediated transport of oxygen and methane is explicitly restricted by the equilibrium concentration of these gases in the soil pores.

In this model configuration, we consider the cotton grass *Eriophorum angustifolium* as the plant species dominating plant-mediated transport in the natural environment conditions of the Chersky floodplain (Kwon et al., 2016). The prescribed constant d_r value is equal to 2 mm, considering a predominance of fine roots, and R_{fr} = 40 % (i.e. from the total available pore-free soil volume, 40 % will be occupied by roots). The model's response to changes in

prescribed values for d_r and f_r is evaluated as part of sensitivity tests described in section 2.2.2.

ii) **Gas transport through the snow**: In this model version, we include the transport of gas through snow during the cold season. Similar to the root exodermis in the plant-mediated transport, the snow is a barrier where gases can move through only by molecular diffusion. Thus, the diffusion of a gas through snow can be related to Fick's first law. The effective diffusion coefficient of a gas species x in snow D_{eff}^{x} (i.e. D_{eff}^{CH4} for methane and D_{eff}^{O2} for oxygen) is related to the dimensionless snow porosity ϕ, the dimensionless tortuosity factor τ, and the diffusion coefficient of the gas in air D_{air}^{x}:

$$D_{eff}^{x} = D_{air}^{x}\, \phi\, \tau \left(\frac{P_0}{P}\right)\left(\frac{T}{T_0}\right)^{1.81} \qquad \text{(S5)}$$

Where $D_{air}^{CH_4}$ = 1.95×10^{-5} m^2 s^{-1} and $D_{air}^{O_2}$ = 1.82×10^{-5} m^2 s^{-1}, both at reference temperature T_0 (273.15 K) and pressure P_0 (1013.3 hPa). The term D_{air}^{x}, should be corrected by the pressure P and the temperature T of the snowpack, as shown in the fourth and fifth terms of Eq. S4 (Mast et al., 1998; Pirk et al., 2016). However, because the model does not explicitly simulate the snowpack thermophysical properties, D_{air}^{x} is not corrected by the P and T values of the snowpack but by those values in the first soil layer. The snow porosity ϕ is the fraction of the snowpack that is occupied by air and is determined by the ratio of the densities of snow (ρ_{snow} = 330 kg/m^3) to ice (ρ_{ice} = 910 kg/m^3) as: $\phi = 1 - \frac{\rho_{snow}}{\rho_{ice}}$ (Wickland et al., 1999). τ is defined as the ratio of the path length in the porous medium over the direct path length (Domine et al., 2008), and is calculated as a function of ϕ (Pirk et al., 2016):

$$\tau = \frac{1-(1-\phi)^{2/3}}{\phi} \qquad \text{(S6)}$$

Thus there will be more tortuosity for the gas molecules as more pore space is available. In reality, D^{x}_{eff} varies through the snow pack in relation to the depth of the snow layer. Chemically reactive gases may undergo adsorption and desorption in the snow grain surface, especially if the snow layer is deep and compacted, allowing gas retention for a period of time in the interstitial space and potential chemical transformation (Domine et al., 2008), thus also affecting the values of D^{x}_{eff}. Here, we simplified the scheme by considering both CH_4 and O_2 as inert gases during their molecular diffusion through the layer of snow with constant ϕ and consequently constant D^{x}_{eff}. For methane, the amount of transferred gas through snow (n^{CH4}_{snow} in mol m^{-2} h^{-1}) is thus represented as:

$$n_{snow}^{CH_4} = D_{eff}^{CH_4} \cdot \left(c^{CH_4} - c_{eq}^{CH_4}\right) \cdot \frac{1}{dz} \cdot dt \qquad \text{(S7)}$$

Where c^{CH4} and $c_{eq}^{CH_4}$ are the methane concentration in the top soil layer and the equilibrium concentration as defined above, and dz is the snow depth. Positive values are emissions of CH_4 into the atmosphere. The same formulation applies for oxygen by replacing the second term with $\left(c_{eq}^{O_2} - c^{O_2}\right)$ due to the sign convention of the gas emissions, leading to positive values, in this case, for oxygen uptake from the atmosphere.

In the model, gases can be transported through a snow layer of defined thickness via snow diffusion (snow threshold depth, h_{snow}). Gas transport through the snow will take place only if $h_{\mathrm{snow}} \geq 5$ cm, while under these conditions, emission, or uptake by other processes is prohibited, following the original JSBACH-methane configuration of Kaiser et al. (2017). Conversely, in summer, transport via diffusion through snow is prohibited when $h_{\mathrm{snow}} < 5$ cm, but transport via ebullition, ordinary molecular diffusion, and plant-mediated transport may take place. As done in the plant-mediated transport, a similar explicit restriction of gas transport is also used here to prohibit the diffusion once the concentration gradient between the soil pore spaces and the atmosphere is zero (i.e. equilibrium conditions). Both h_{snow} and ϕ are parameters in the model used to restrict the transport of gas via diffusion through snow during the cold season, and assessments of the model sensitivity to changes in the values of these parameters were done in this work.

iii) **Order of emission processes**: In the JSBACH-methane module, the transport pathways occur sequentially, i.e. one after the other, taking care of mass conservation during each model iteration. In the original model version, the order of the transport pathways was: ebullition, molecular diffusion and plant-mediated transport. This order was set by taking the relative speed of each process into consideration, with ebullition as the fastest process and plant-mediated transport as the slowest due to the resistance of gas to diffuse through the plants exodermis. In contrast, in this model configuration, the order of processes is: plant-mediated transport, molecular diffusion, and ebullition. This new order of processes was chosen by taking their expected share in the total emissions into consideration and was done mainly to improve the small contribution that plant-mediated transport had in the original JSBACH-methane module. The aerenchyma structures of plants in wetlands are an efficient exit route for CH_4 to the atmosphere, bypassing zones of aerobic oxidation. Previous studies have demonstrated that in the presence of vascular plants in Arctic permafrost tundra ecosystems, plant-mediated transport is the dominating methane transport pathway over ebullition and diffusion (Knoblauch et al., 2016), and this transport pathway can contribute from 30 to 100 % to the total CH_4 flux (Bridgham et al., 2013).

Molecular diffusion is in the second position of the methane transport pathways. Despite the fact that in nature the amount of methane emitted through this pathway is lower than that emitted via ebullition and plant transport, it takes place throughout the year and is not limited by other factors such as plant root tissues. Finally, ebullitive methane fluxes were considered in the last position of the sequence of CH_4 transport processes in the model. The amount of methane emitted via ebullition can be significant and can exceed by orders of magnitude the amount of gas emitted via plants and by molecular diffusion (e.g. Tokida et al., 2007). However, ebullition is a rapid process that is highly variable temporally and spatially. Observations have shown that CH_4 emitted through ebullition occurs sporadically and mainly in undisturbed natural water bodies, such as lakes and ponds, where gas bubbles formed during active methanogenesis ascend rapidly through the water and into the atmosphere, circumventing aerobic soil layers (Klapstein et al., 2014; Knoblauch et al., 2016). Thus, by leaving this process in the last position we ensured that the small amounts of CH_4 transported by molecular diffusion can work properly. In contrast, gas transport via diffusion through the snow will take place under conditions of considerably high snow depth aboveground as discussed above in point ii) of this section, and thus does not compete with the other transport processes. Due to the structure of the model, it is not possible to run parallel processes and instead, a sequential flow of processes has to be computed which is also cost effective. Since this modification is solely based on computational design, a sensitivity test to account for uncertainties due to having different sequence of methane transport pathways is not desirable.

References

Bridgham, S. D., Cadillo-Quiroz, H., Keller, J. K., and Zhuang, Q.: Methane emissions from wetlands: biogeochemical, microbial, and modeling perspectives from local to global scales, Global Change Biology, 19, 1325-1346, 2013, 10.1111/gcb.12131.

Domine, F., Albert, M., Huthwelker, T., Jacobi, H.-W., Kokhanovsky, A. A., Lehning, M., Picard, G., and Simpson, W. R.: Snow physics as relevant to snow photochemistry, Atmospheric Chemistry and Physics, 8, 171-208, 2008, 10.5194/acp-8-171-2008.

Kaiser, S., Göckede, M., Castro-Morales, K., Knoblauch, C., Ekici, A., Kleinen, T., Zubrzycki, S., Sachs, T., Wille, C., and Beer, C.: Process-based modelling of the methane balance in periglacial landscapes (JSBACH-methane), Geoscientific Model Development, 10, 333-358, 2017, 10.5194/gmd-10-333-2017.

Kirkby, M. J.: Hydrograph modelling strategies. In: Process in Physical and Human Geography, Peel, R., Chisholm, M., and Hagget, P. (Eds.), Heinemann, London, 1975.

Klapstein, S. J., Turetsky, M. R., McGuire, D., Harden, J. W., Czimiczik, C. I., Xu, X., Chanton, J. P., and Waddington, J. M.: Controls on methane released through ebullition in peatlands affected by permafrost degradation, Journal of Geophysical Research: Biogeosciences, 119, 418-431, 2014, 10.1002/2013JG002441.

Knoblauch, C., Spott, O., Evgrafova, S., Kutzbach, L., and Pfeiffer, E.-M.: Regulation of methane production, oxidation, and emission by vascular plants and bryophytes in ponds of the northeast Siberian polygonal tundra, Journal of Geophysical Research: Biogeosciences, 120, 2525-2541, 2016, 10.1002/2015JG003053.

Kutzbach, L., Wagner, D., and Pfeiffer, E.-M.: Effect of microrelief and vegetation on methane emission from wet polygonal tundra, Lena Delta, Northern Siberia, Biogeochemistry, 69, 341-362, 2004, 10.1023/B:BIOG.0000031053.81520.db.

Kwon, M. J., Beulig, F., Ilie, I., Wildner, M., Küsel, K., Merbold, L., Mahecha, M. D., Zimov, N., Zimov, S. A., Heimann, M., Schuur, E. A., Kostka, J. E., Kolle, O., Hilke, I., and Göckede, M.: Plants, microorganisms, and soil temperatures contribute to a decrease in methane fluxes on a drained Arctic floodplain, Global Change Biology, 23, 2396-2412, 2016, 10.1111/gcb.13558.

Marthews, T. R., Dadson, S. J., Lehner, B., Abele, S., and Gedney, N.: High-resolution global topographic index values for use in large-scale hydrological modelling, Hydrology and Earth System Sciences, 19, 91-104, 2015, 10.5194/hess-19-91-2015.

Mast, M. A., Wickland, K. P., Striegl, R. T., and Clow, D. W.: Winter fluxes of CO_2 and CH4 from subalpine soils in Rocky Mountain National Park, Colorado, Global Biogeochemical Cycles, 12, 607-620, 1998, 10.1029/98GB02313.

Pirk, N., Tamstorf, M. P., Lund, M., Mastepanov, M., Pedersen, S. H., Mylius, M. R., Parmentier, F.-J. W., Christiansen, H. H., and Christensen, T. R.: Snowpack luxes of methane and carbon dioxide from high Arctic tundra, Journal of Geophysical Research: Biogeosciences, 121, 2016, 10.1002/2016JG003486.

Sivapalan, M., Beven, K., and Wood, E. F.: On hydrologic similarity 2. A scaled model of storm runoff production, Water Resources Research, 23, 2266-2278, 1987, 10.1029/WR023i012p02266.

Tokida, T., Mizoguchi, M., Miyazaki, T., Kagemoto, A., Nagata, O., and Hatano, R.: Episodic release of methane bubbles from peatland during spring thaw, Chemosphere, 70, 165-171, 2007, 10.1016/j.chemosphere.2007.06.042.

Wickland, K. P., Striegl, R. G., Schmidt, S. K., and Mast, M. A.: Methane flux in subalpine wetland and unsaturated soils in the southern Rocky Mountains, Global Biogeochemical Cycles, 13, 101-113, 1999, 10.1029/1998GB900003.

Section 2. Figures in supplementary material

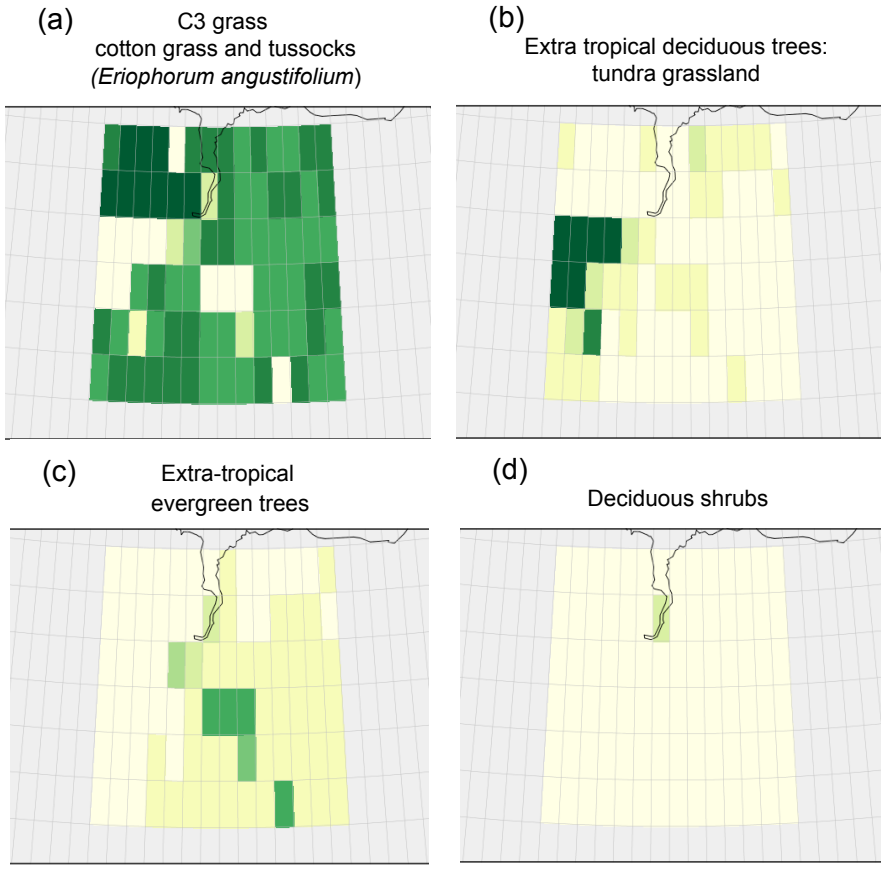

Figure S1 – Spatial distribution of the four land cover types present in the model domain: a) C3 grasses with 66 % coverage in the wetter areas in the northwest, b) Deciduous trees with 19 % coverage and characteristic of the drier tundra grassland located in the central west region of the domain, c) Evergreen trees with 14 % coverage mostly present in the central and southeast parts of the domain in the driest regions, and d) Deciduous shrubs with 1 % coverage only present in one grid cell located in the north central part of the model domain near Chersky.

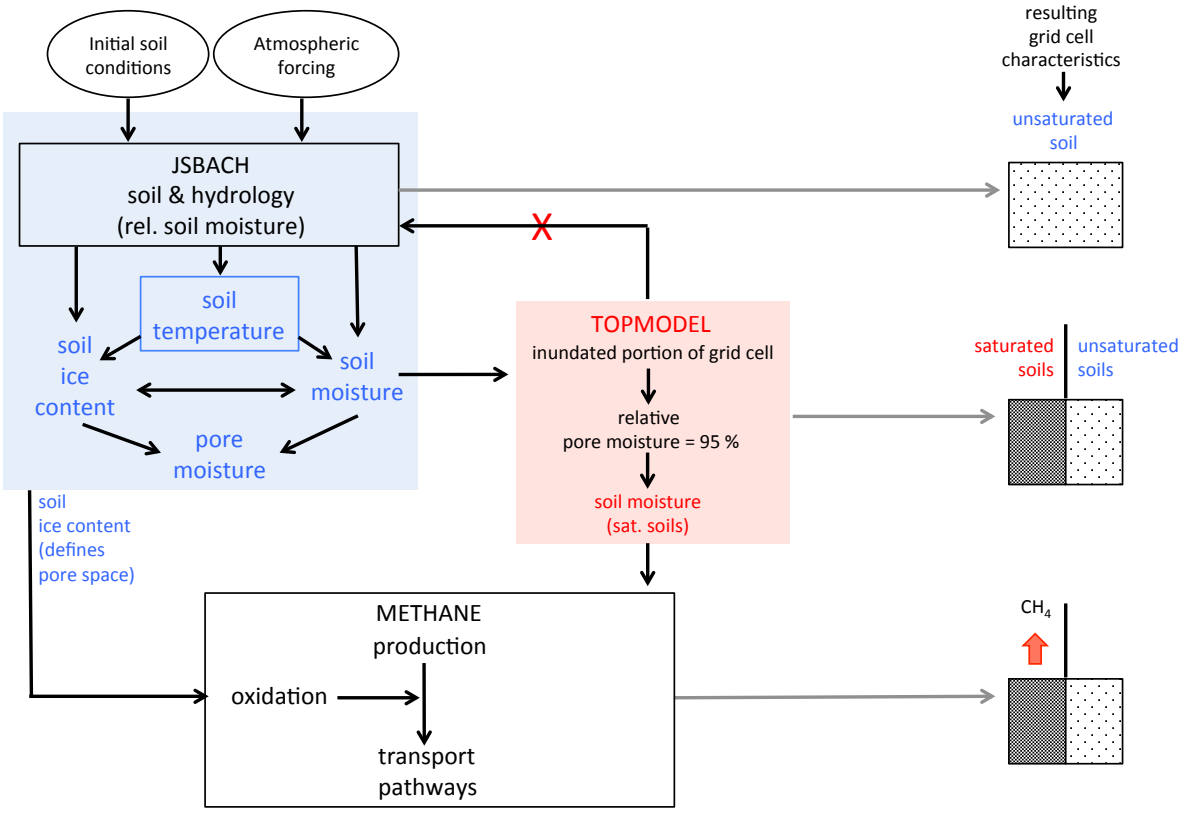

240 **Figure S2** – Schematic representation of the connections between the hydrology and soil schemes, and TOPMODEL approach, in the JSBACH-methane model. The blue text represents those variables that are not influenced by the TOPMODEL approach, which is represented within a red box. The production, oxidation, and transport of methane take place only in the water-saturated portion of the grid cell.

245

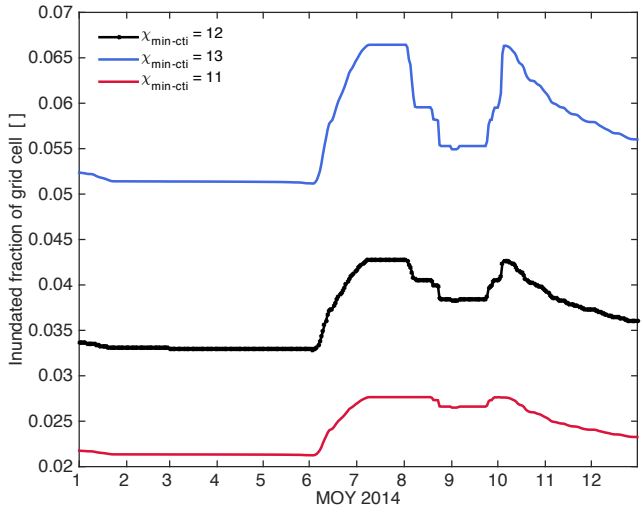

250

255

260

Figure S3 – Comparison of the temporal change of the daily mean inundated areas in the model domain during 2014, due to the definition of three different values of χ_{min_cti} during sensitivity tests.

265

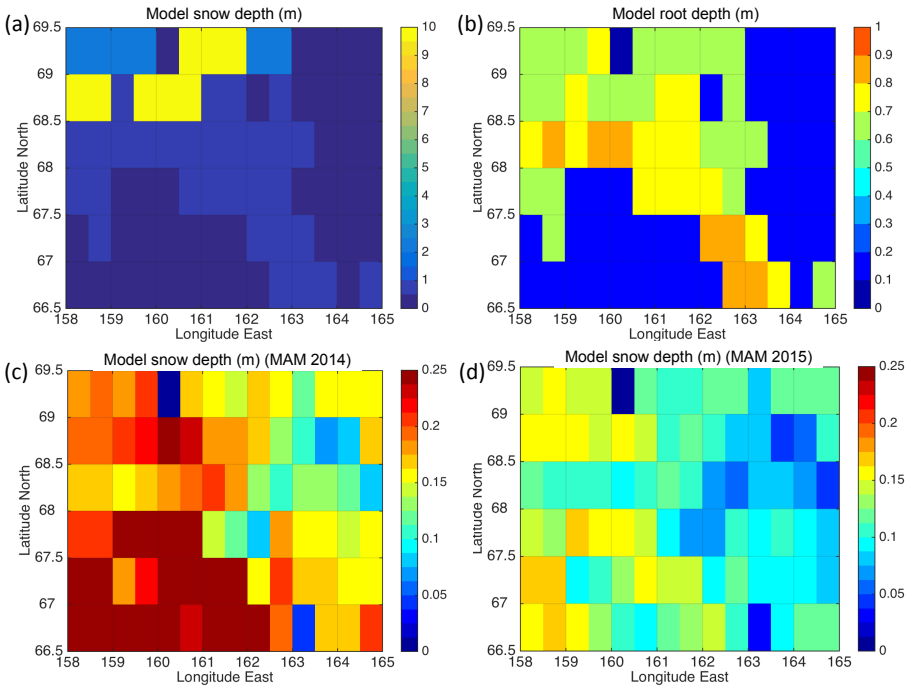

Figure S4 – Spatial distribution of soil input parameters and calculated mean spring snow depth: a) spring snow depth in 2014 and b) spring snow depth in 2015; c) soil depth, d) maximum root depth.

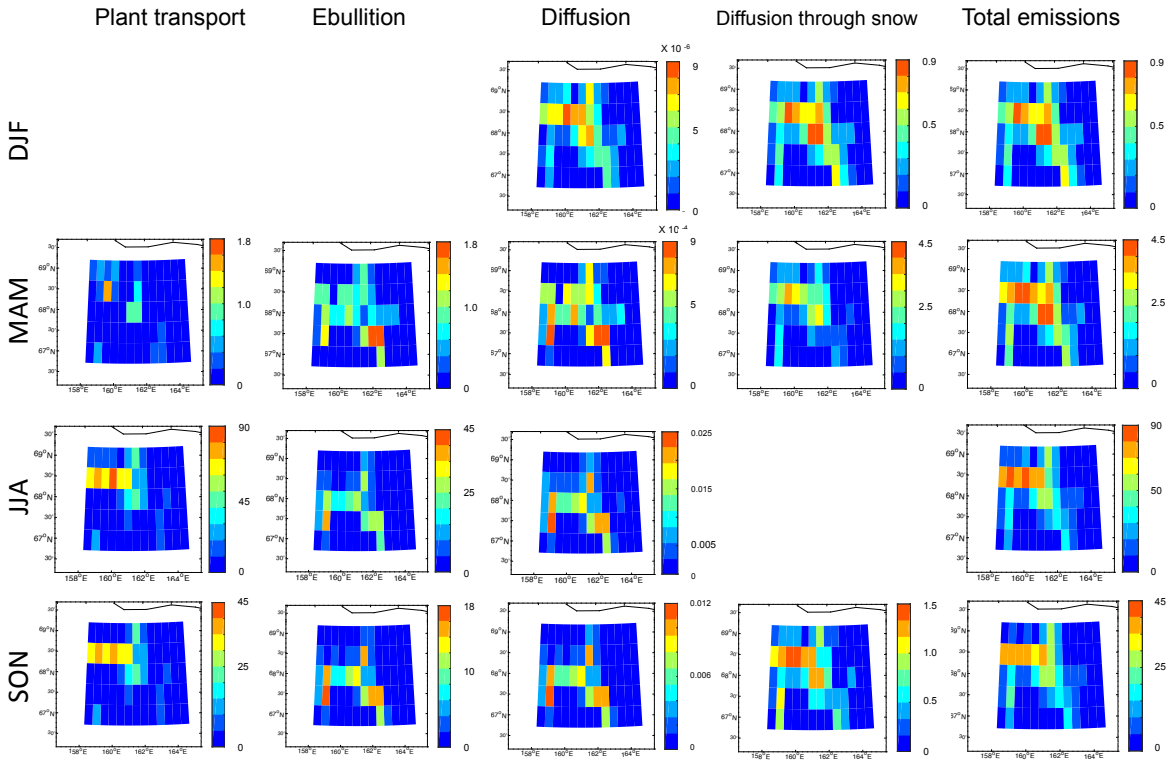

Figure S5 – Spatial distribution of methane emissions due to the individual pathways and the total in the model domain through seasons. Due to the contrastingly different magnitude of emissions between the individual pathways, the color bars are not equal between the figures, thus this figure is only to visually depict the spatial distribution of the emissions within the domain.

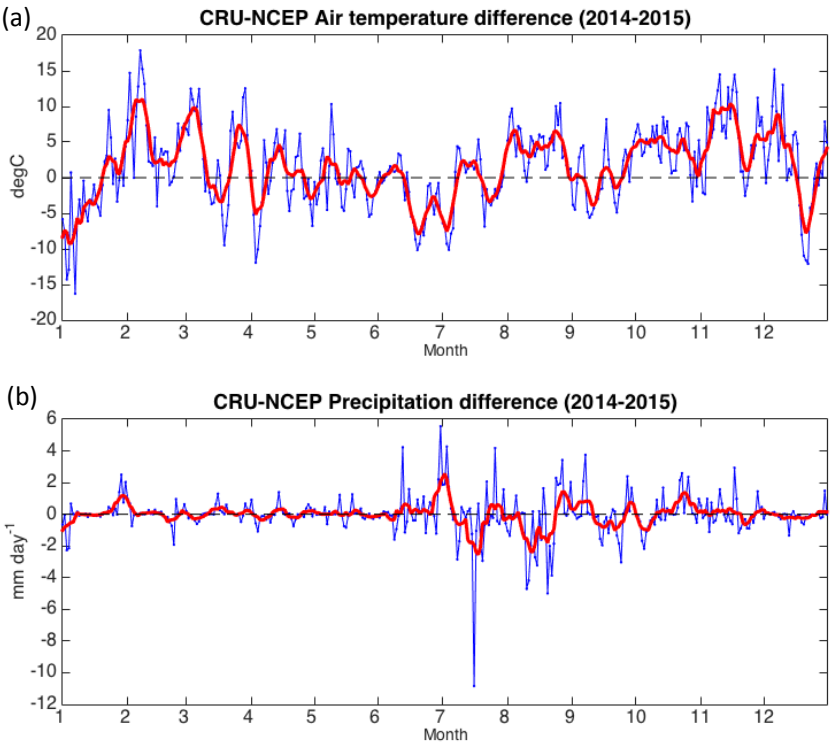

Figure S6 – Difference between 2014 and 2015 of the mean values of the CRU-NCEP data a) air temperature and b) precipitation in the model domain. The blue line shows daily values and the red line is the three-day running mean.

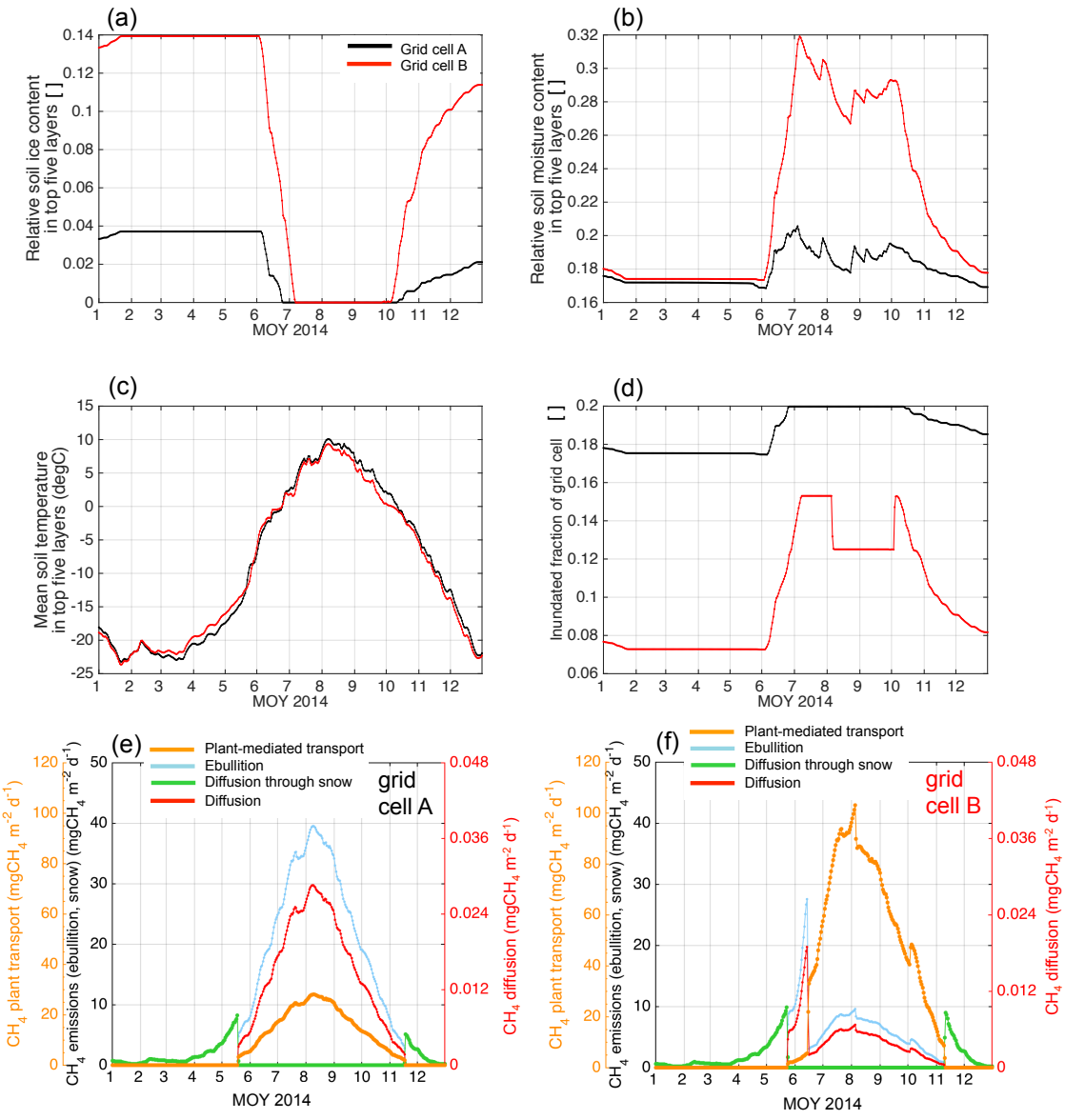

Figure S7 - Time series of mean daily values for ancillary variables and methane emissions via individual pathways for the grid cells A and B during 2014: a) mean relative soil ice content in the top five layers, b) mean relative soil moisture content in the top five layers, c) mean soil temperature in the top five layers, d) inundated fraction of the grid cell, and methane emissions for: e) grid cell A and f) grid cell B.

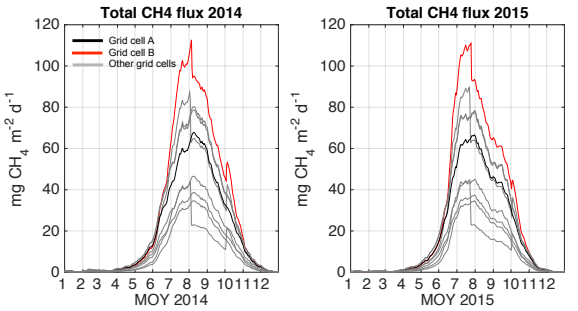

JJA, 2014 (mean ± 1σ)

25±-7	56±-12	24±-4
73±-16	49±-5	28±-4
57±-7	58±-7	33±-5

JJA, 2015 (mean ± 1σ)

25±-8	57±-15	25±-5
75±-18	50±-7	28±-5
59±-9	59±-10	34±-6

Figure S8 – Time series of daily total modeled CH_4 fluxes for 2014 and 2015 in nine model grid cells, eight of them surrounding grid cell A of Fig. 1. The tables below contain the mean ± 1σ fluxes for June, July and August for a each model grid cell.